Available online at https://sextante-ensb.com

Revista Sextante

ISSN : 2665-3923

Volume: 34 Issue: 01 (2026)

Performance and Analysis of Methylammonium Lead Bromide ($MAPbBr_3$) Solar Cell

Ashfaq Nabi[a]*, Mehmood Ullah Shah[b]

a. *Corresponding Author: MS Student, Department of U.S Pakistan Center for Advanced Studies in Energy, University of Engineering and Technology Peshawar, Pakistan (ashfaqnabi@uetpeshawar.edu.pk)*
b. *MS Student, Department of U.S Pakistan Center for Advanced Studies in Energy, University of Engineering and Technology Peshawar, Pakistan*

Article History
Received September 08th, 2026
Accepted November 3rd, 2026
Published November 16th, 2026

© 2026 The Authors. This article is an Open Access article distributed under the terms and conditions of the Creative Commons Attribution(CC-BY)license https://creativecommons.org/licenses/by/4.0

Abstract
Wide-band-gap perovskites such as methylammonium lead bromide ($MAPbBr_3$) are attractive for semi-transparent, and indoor photovoltaics because of their high open-circuit voltage and good stability. In this work, an all-inorganic planar FTO/Nb_2O_5/$MAPbBr_3$/Cu_2O/Au solar cell was designed and numerically simulated using OghmaNano, which solves the Poisson and drift-diffusion equations with Shockley-Read-Hall recombination. The effects of absorber thickness, electron transport layer (ETL) and hole transport layer (HTL) thickness, absorber and transport-layer doping, absorber defect density, and operating temperature on the current density-voltage characteristics and quantum efficiency were systematically investigated. The optimized device used a 600 nm absorber, a 170 nm Nb_2O_5 ETL, and a 110 nm Cu_2O HTL, with doping concentrations of 1×10^{20} m^{-3} (absorber), 1×10^{21} m^{-3} (ETL), and 1×10^{24} m^{-3} (HTL), a defect density of 1×10^{19} m^{-3}, and an operational temperature of 300 K. Under AM 1.5G irradiance, this device attained a PCE efficiency of 10.29%, an open-circuit voltage of 1.62 V, a short-circuit current density of 10.39 mA/cm², and a FF of 61%. These results show that Nb_2O_5 and Cu_2O are promising inorganic transport layers for efficient and stable wide-band-gap perovskite solar cells.

Keywords: Wide-band-gap perovskites; Methylammonium lead bromide ($MAPbBr_3$); Perovskite solar cells; Niobium pentoxide (Nb_2O_5); Cuprous oxide (Cu_2O); OghmaNano simulation; Electron transport layer; Hole transport layer; Power conversion efficiency (PCE); Numerical device optimization.

1. Introduction

The increasing global claim for clean and affordable energy has driven intensive investigation into next-generation photovoltaic technologies. Among them, organic-inorganic halide perovskites have emerged as the front runners due to their high absorption coefficients, long carrier diffusion lengths, and low-cost elucidation Formability [1]. In under ten years, efficiencies of perovskite solar cells (PSCs) have grown from several percent to near-commercial values rivaling silicon [2]. Most of this success, however, has been achieved on iodide-based perovskites like methylammonium lead iodide ($MAPbI_3$), which has a band gap of 1.55 eV that is well matched to the solar spectrum. Conversely,

© 2026 The Authors. This article is an Open Access article distributed under the terms and conditions of the Creative Commons Attribution(CC–BY)license
https://creativecommons.org/licenses/by/4.0

methylammonium lead bromide ($MAPbBr_3$) has a larger band gap of 2.26 eV [3]. This makes it unsuitable for single-junction cells with the goal of maximum efficiency but attractive for other applications. Its wide band gap results in a high open-circuit voltage, rendering it an interesting candidate as a top-cell absorber in a tandem architecture, semi-transparent photovoltaics, as a building-integrated and indoor/hybrid light harvester [4, 5]. $MAPbBr_3$ is also generally more moisture- and structure-stable than its iodide equivalent.

The enactment of a perovskite solar cell be contingent strongly on its charge transport layers. Organic hole carrying resources such as Spiro-OMeTAD are widely used, but they are expensive, require hygroscopic dopants, and degrade under heat and humidity, which limits long-term stability [6]. Inorganic alternatives are therefore being explored. Cuprous oxide (Cu_2O) is a p-type semiconductor that is abundant, non-toxic, low-cost, and has good hole mobility, making it a suitable inorganic hole transport layer (HTL) [7]. On the electron side, niobium pentoxide (Nb_2O_5) is a wide-band-gap n-type oxide with good chemical stability and favourable conduction band alignment, and it has been investigated as an alternative to TiO_2 as an electron transport layer (ETL) [8]. Combining these two layers with a $MAPbBr_3$ absorber gives an all-inorganic transport scheme, $FTO/Nb_2O_5/MAPbBr_3/Cu_2O/Au$, which is attractive for low-cost and stable devices.

Optimising such a multilayer structure by experiment alone is time-consuming, since many parameters are strongly coupled. Numerical simulation offers a practical and low-cost route to understand the underlying physics and to guide fabrication. In this work, we use the OghmaNano software (formerly gpvdm) to model the $FTO/Nb_2O_5/MAPbBr_3/Cu_2O/Au$ solar cell. OghmaNano is a general-purpose device simulator that resolves the Poisson equation and the e and h drift-diffusion and continuity equations, together with optical modelling of multilayer stacks and Shockley-Read-Hall recombination through trap states [9]. We systematically study the effect of layer thickness, doping concentration, on the current density-voltage (J-V) Property and the crucial photovoltaic factors (open-circuit voltage, short-circuit current density, fill factor, and PCE). Because solar cells operate at elevated temperatures under illumination, we also examine the influence of operating temperature on scheme enactment and stability. From these outcomes, we identify an optimised device configuration and discuss the physical mechanisms behind the observed trends, providing design guidelines for proficient and established wide-band-gap perovskite solar cells.

2. Device Design and Simulation Methodology

The solar cell device simulator OghmaNano (version 8.1.093) was used for the simulation. The model follows the effective medium approximation to the performance of the optoelectronic and the photovoltaic devices. A finite difference numerical method numerically solves the equations of its model [9-11]. In this model, the Poisson equation is solved explicitly for the prospective dissemination in the device arrangement from x = 0 (transparent conductive oxide) to x = t (back metal contact) where t is the total thickness of the device.

$$\frac{d}{dx}\epsilon_o\varepsilon_r\frac{d\varphi}{dx} = q(n-p) \quad (1)$$

The permittivity of free space is denoted as ϵ_o , while the relative permittivity of $CH3NH3PbBr_3$ is ε_r , q represents the fundamental charge, n indicates the electron carrier density, and p signifies the hole carrier density. To obtain the electron current density (Jn) and hole current density (Jp), the continuity equations (2) and (3) are resolved, correspondingly.

$$\frac{dJn}{dx} = q\left(Rn - Gn + \frac{\partial n}{\partial t}\right) \quad (2)$$

$$\frac{dJp}{dx} = p\left(Rp - Gp + \frac{\partial p}{\partial t}\right) \quad (3)$$

The generation rates of free e and h are represented by Gn and Gp, whereas Rn and Rp indicates the recombination rate of electrons and holes. The drift-diffusion equations for electrons and holes are addressed as (4) and (5), respectively.

$$J_n = q\mu_e n\frac{\partial E_{LUMO}}{\partial x} + qD_n\frac{\partial n}{\partial x} \quad (4)$$

$$J_p = q\mu_p p\frac{\partial E_{HOMO}}{\partial x} + qD_p\frac{\partial p}{\partial x} \quad (5)$$

© 2026 The Authors. This article is an Open Access article distributed under the terms and conditions of the Creative Commons Attribution(CC–BY)license
https://creativecommons.org/licenses/by/4.0

The band-gap (Eg) is the energy variance among the highest occupied molecular orbital (E_{HOMO}) and the lowest unoccupied molecular orbital (E_{LUMO}) of the active layer (CH3NH3PbBr3). The electron and hole mobility is denoted by μ_e and μ_p, where D_n and D_p represent the electron and hole diffusion coefficients, correspondingly.

The software application employs the Shockley-Read-Hall (SRH) model to replicate the recombination, trapping, and detraping of both e and h in the active layer. The standard factors employed for the SRH model are enumerated in Table 1. The transfer matrix model is employed in the database to account for the optical absorption effects of various layers, the reflection of incident light from these layers, and the transmission of light through the device stack, under the assumption of normal light incidence.

The structure of the plane device can be realized from Figure 1. The device comprises a transparent conductive oxide (FTO-cathode) for light passage and electron collection. Cuprous oxide (Cu_2O) and niobium pentoxide (Nb_2O_5) layers serve for hole or electron transport to electrodes. The photon-absorbing layer was CH3NH3PbBr3 ($MAPbBr_3$), and Au is the hole-collecting anode. The thicknesses of the ETL, active layer, and HTL are specified as 170, 600, and 110 nm, respectively.

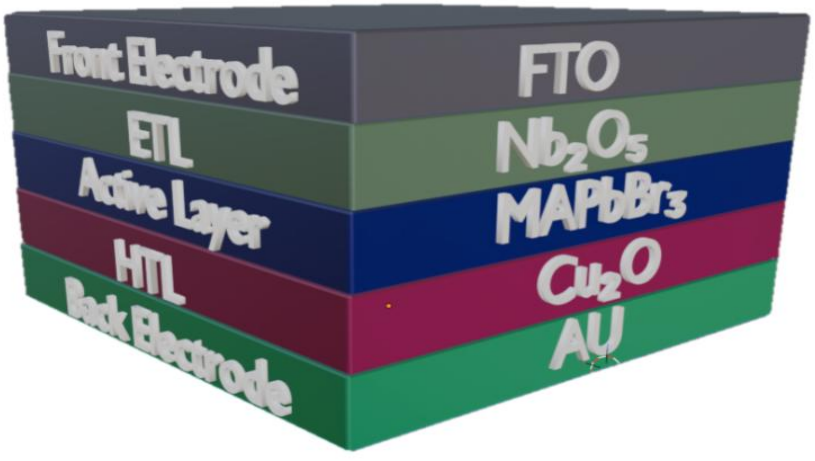

Figure 1. Schematic of the proposed FTO/Nb2 O5 /MAPbBr3 /Cu2 O/Au perovskite solar cell structure.

Table 1. Shockley-Read-Hall (SRH) Factors [12].

Parameters	Values
Electron trap density ($m^{-3}eV^{-1}$)	$1x10^{22}$
Hole trap density ($m^{-3}eV^{-1}$)	$1x10^{22}$
Electron/hole tail slope (eV)	0.06
Free electron to trapped electron (m^2)	$1x10^{-21}$
Free hole to trapped electron (m^2)	$1x10^{-22}$
Free electron to trapped hole (m^2)	$1x10^{-22}$
Free hole to trapped hole (m^2)	$1x10^{-21}$
Number of trap bands	5

The optical absorption and the refractive indices of the resources considered in our device model are obtained from OghmaNano's internal catalogue. Other electrical, optical, and DOS properties of the materials are taken from [13-15] and are summarized in Table 2.

© 2026 The Authors. This article is an Open Access article distributed under the terms and conditions of the Creative Commons Attribution(CC–BY)license
https://creativecommons.org/licenses/by/4.0

Table 2. Material factors used in the simulation

Parameters	Nb_2O_5	$MAPbBr_3$	Cu_2O
Thickness (nm)	170	600	110
Bandgap (eV)	3.4	2.26	2.17
Electron Affinity (eV)	3.9	3.7	3.2
Dielectric permittivity	9	7.5	7.1
CB density of states (m^{-3})	3.7×10^{24}	3.5×10^{25}	2.5×10^{26}
VB density of states (m^{-3})	1.8×10^{25}	4×10^{25}	2.5×10^{26}
Electron mobility ($m^2 V^{-1} s^{-1}$)	1×10^{-2}	24×10^{-4}	2×10^{-2}
Hole mobility ($m^2 V^{-1} s^{-1}$)	2.5×10^{-3}	24×10^{-4}	8.6×10^{-1}
Donor density N_D (m^{-3})	$1x10^{21}$	-	-
Acceptor density N_A (m^{-3})	-	$1x10^{19}$	$1x10^{24}$
Defect density (m^{-3})	$1x10^{16}$	$1x10^{20}$	$1x10^{16}$

3. Results and Discussion

3.1. JV Characteristics and Quantum Efficiency

Figure 2(a) shows the J-V characteristics of the proposed Nb2 O5 /MAPbBr3 /Cu2 O solar cell under AM 1.5G illumination. The device shows a short circuit current density (Jsc) of 10.39 mA/cm² and an open circuit voltage (Voc) of 1.62 V. The large band gap $MAPbBr_3$ and the good band alignment of Nb2O5 with hole and electron transport layers Cu_2O allow carriers to be extracted efficiently with high Voc and low interfacial recombination.

Figure 2(b) shows the QE spectrum of the scheme. The QE of the cell is high 90% in the range of 400-650 nm, signifying efficient absorption of photons and corresponding collection of the carriers in the spectral region. The spectral oscillations arise from the optical interference in the thin layers of the device. QE also drops quickly beyond 760 nm.

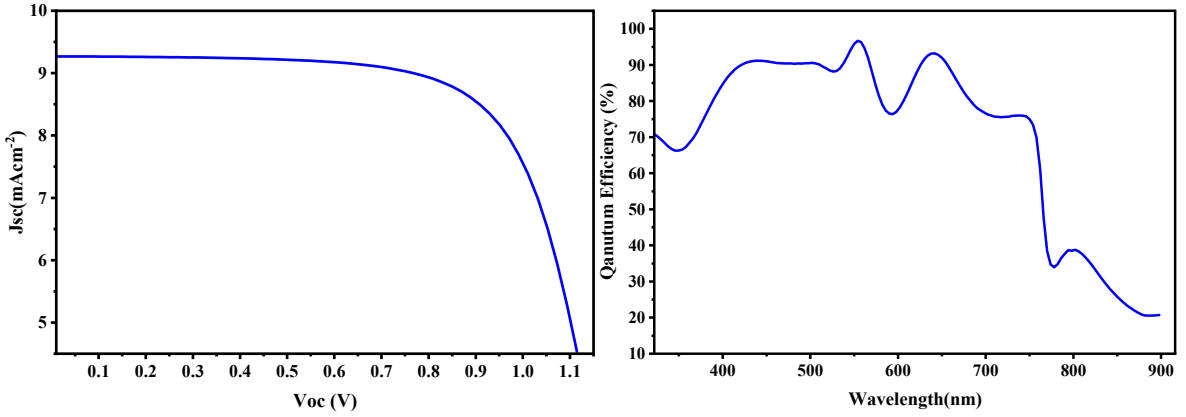

Figure 2: (a) J-V characteristics and (b) quantum efficiency of the Nb2 O5 /MAPbBr3 /Cu2 O perovskite solar cell.

3.2. Optimization of Active Layer, Charge Transport Layer Thickness

The thickness of the active layer is an imperative operational factor to absorb, generate, and perform charge transport in the solar cell. Absorber thickness variation is achieved by fluctuating thickness values from 100 to 800 nm in steps of 50 nm keeping other scheme factors as mentioned in Table 2 persistent.

PCE, FF, and Jsc rise with a rise in absorber thickness as revealed in Figure 3. As the active layer thickness rises, more photons are captivated, generating more charge carriers, and thus Jsc is higher. It also reduces the effective band

© 2026 The Authors. This article is an Open Access article distributed under the terms and conditions of the Creative Commons Attribution(CC–BY)license
https://creativecommons.org/licenses/by/4.0

gap, thus enhancing the absorption of lengthier wavelength photons[16, 17]. The low thickness cannot absorb the low-energy longer-wavelength photons. Therefore, the absorber should have an appropriate thickness. However, the absorption efficiency depends on the diffusion length and the absorption coefficient of the absorbing material. If the absorber thickness exceeds the diffusion length of carriers, the carriers fail to grasp the CTL and recombine, thus degrading the performance[18]. The absorber can have a thickness up to the diffusion length of the material. The peak results for absorber thicknesses are presented in Table 2.

Primarily defining the active layer thickness at 600 nm, the thickness of the Nb_2O_5 electron transport layer (ETL) was initially tuned. The CTL (ETL and HTL) in photovoltaic cells functions not only to facilitate charge transport from the active layer to the corresponding electrodes but also acts as a separating layer between the absorber and the electrodes[19]. The ETL and HTL thickness was refined by adjusting it between 50 nm and 170 nm while maintaining constant absorber and HTL thickness. After establishing the ideal thickness for the ETL, the HTL thickness was refined while maintaining the improved thickness values for both the ETL and absorber.

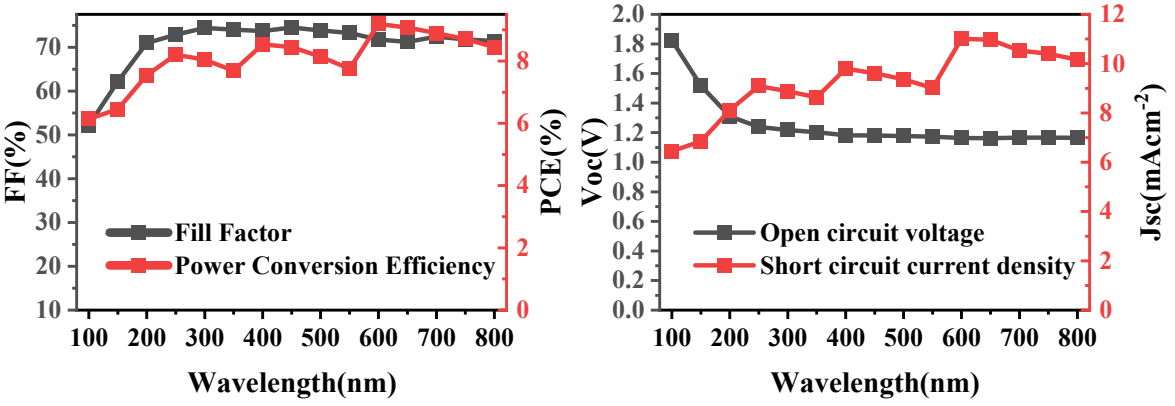

Figure 3. Impact of absorber thickness on (a) FF and PCE, (b) Voc and Jsc

In n-i-p planar solar cells, the front layer, ETL, significantly influences performance, which improves with more thickness. The decline in performance is attributed to the reduction in clearness with increased thickness. The thickness of HTL has a negligible impression on the enactment of solar cells, as illustrated in the Figure 5(b). For all computations, the ETL thickness is maintained at 170 nm to fulfil the objective of layer separation in Figure 4. Augmenting the thickness of the HTL elevates the series resistance among the absorber and HTL, which consequently diminishes Voc and causes a fall in FF, Jsc, and PCE; thus, the optimal thickness for HTL is 110 nm as illustrated in Figure 5.

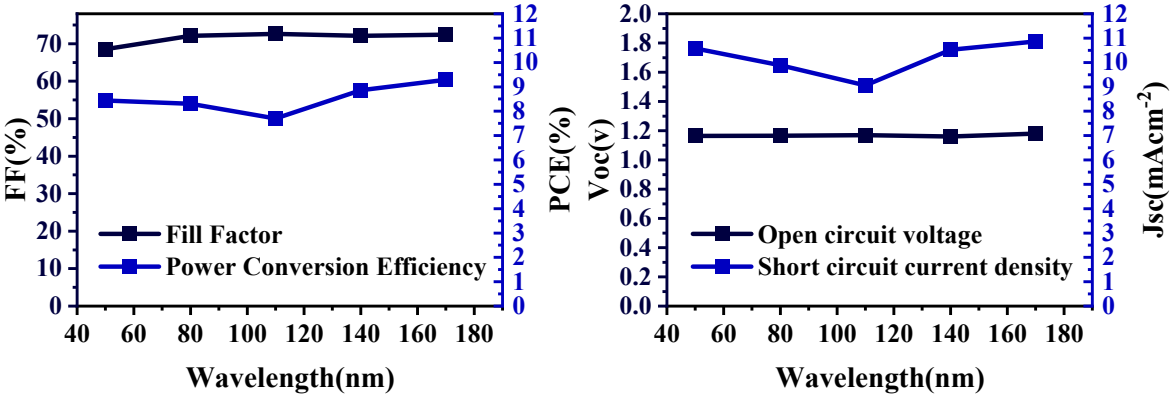

Figure 4. Impact of ETL thickness on (a) FF and PCE, (b) Voc and Jsc

© 2026 The Authors. This article is an Open Access article distributed under the terms and conditions of the Creative Commons Attribution(CC–BY)license
https://creativecommons.org/licenses/by/4.0

3.3. Optimization of Absorber Layer, Charge Transport Layer Doping

To examine the optimization of absorber doping, the acceptor doping density N_A changes from 10^{18} to 10^{24} m^{-3}, ensuring that the active layer and CTLs remain at their optimal thicknesses. Absorber doping enhances solar cell efficiency by boosting the concentration of prevalent charge carriers, thus enhancing conductivity and diminishing the recombination rate[20, 21].

Figure 6(a) depicts a decline at 10^{20} m^{-3}, where a dramatic decrease is noted, suggesting that higher doping levels lead to dominant Auger recombination. Higher N_A results in a reduction of charge transport and a decline in charge mobilities (μn and μp) attributed to heightened ionized impurity scattering [22].

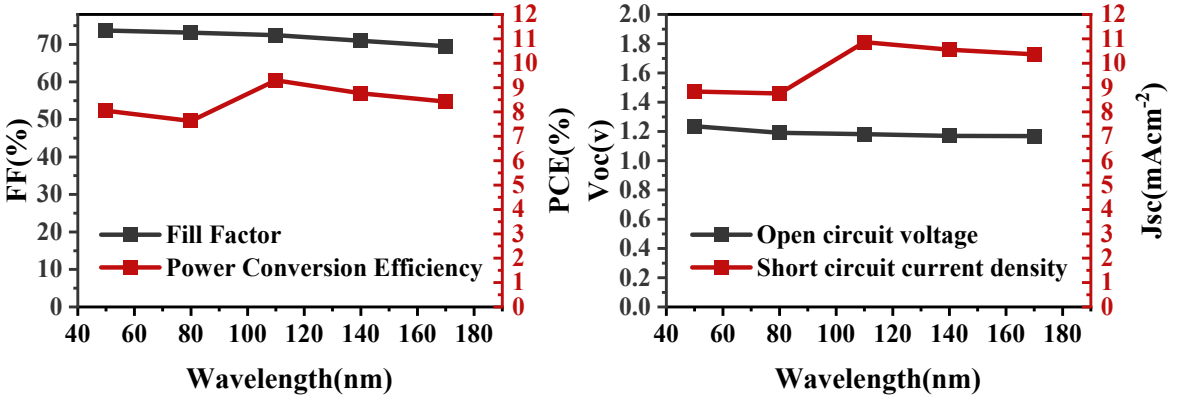

Figure 5. Impact of HTL thickness on (a) FF and PCE, (b) Voc and Jsc

The abrupt rise in Voc in most cells at elevated doping levels (exceeding 10^{24} m^{-3}) leads the absorber to lose its semiconductor characteristics and acquire metallic traits as seen in Figure 6(b). The best doping level of 10^{20} m^{-3} was chosen for all the cells absorbers.

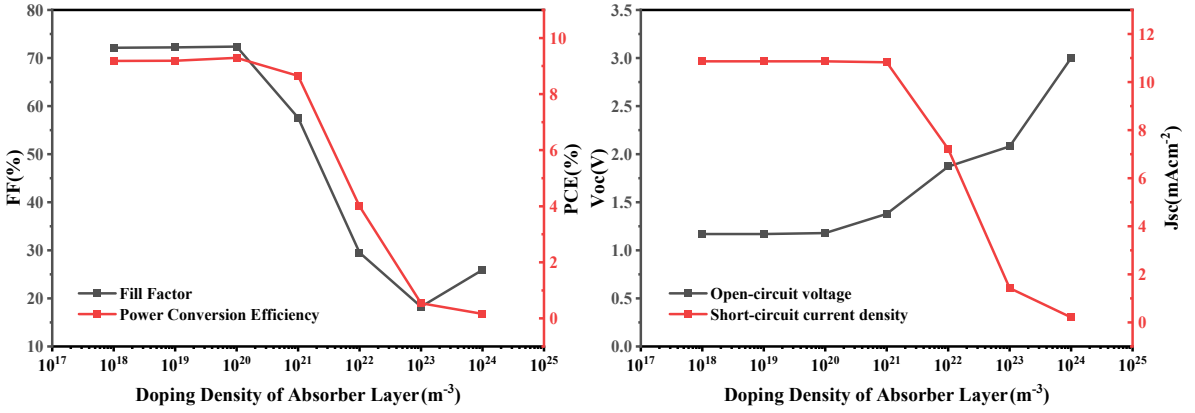

Figure 6. Impact of absorber doping on (a) FF and PCE (b) Voc and Jsc

© 2026 The Authors. This article is an Open Access article distributed under the terms and conditions of the Creative Commons Attribution(CC–BY)license
https://creativecommons.org/licenses/by/4.0

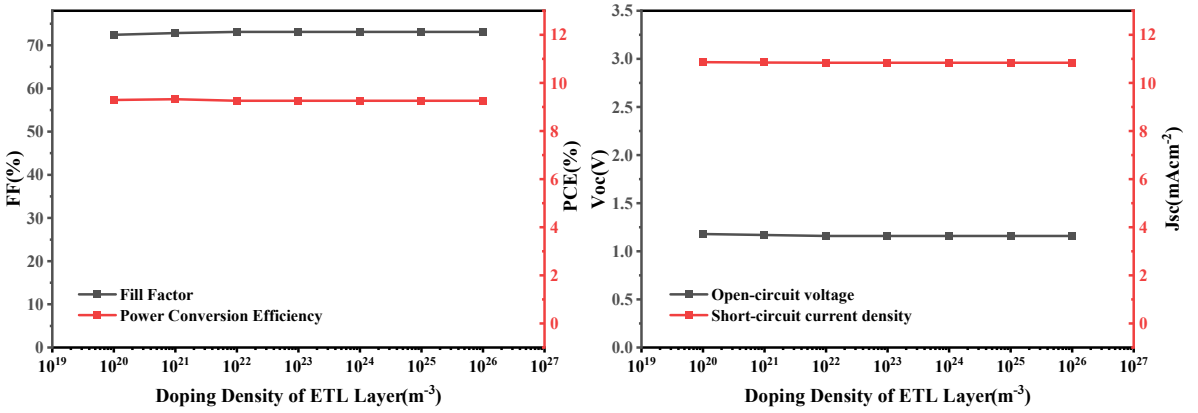

Figure 7. Impact of ETL doping on (a) FF and PCE (b) Voc and Jsc

After performing an improvement of absorber doping, the refinement of the electron transport layer and hole transport layer is conducted. The doping concentration of the electron transport layer (ETL) (N_D) and the hole transport layer (HTL) (N_A) ranges from 10^{20} to 10^{26} m^{-3}. The doping of CTL enhances charge conductivity by augmenting the electric field at the interface between the absorber and CTL. The augmentation of doping elevates the Fermi level disparity at the active/CTL interface, hence generating a robust electric field that enhances charge transport to the corresponding electrodes [23]. The electric field at the ETL/active boundary aids in the extraction of electrons, hence promoting the movement of electrons (predominant charge carriers) while obstructing holes (subordinate charge carriers). In a similar manner, the electric field at the active/HTL interface draws holes (the predominant charge carriers) near the HTL while pushing away the electrons.

Figure 7 illustrate that the performance is nearly constant with ETL doping concentration. The augmentation in PCE, and Jsc as a consequence of heightened HTL doping is illustrated in Figure 8. The optimal values for CTLs (ETL and HTL) are considered to be 10^{21} and 10^{24} m^{-3}.

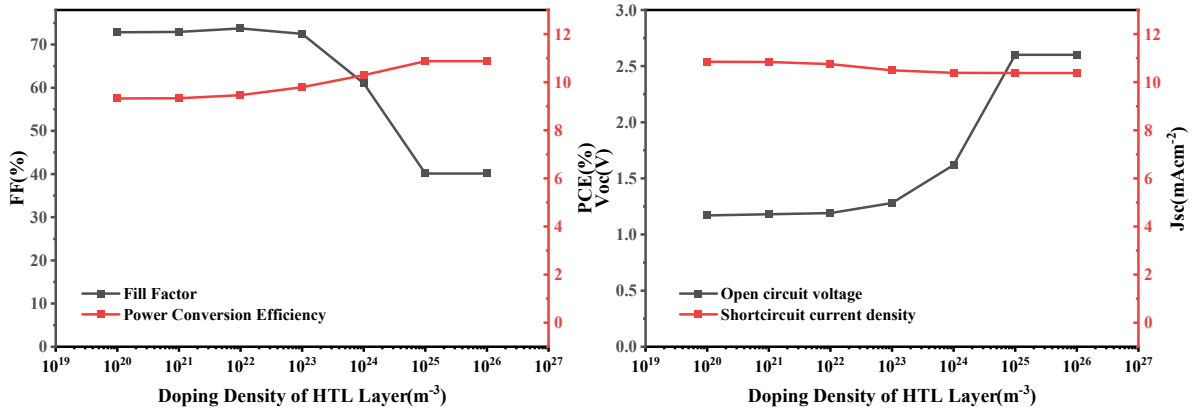

Figure 8. Impact of HTL doping on (a) FF and PCE (b) Voc and Jsc

4. Conclusion

In this work, an inorganic FTO/Nb_2O_5/$MAPbBr_3$/Cu_2O/Au perovskite solar cell was designed and numerically optimized using OghmaNano. The effects of layer thickness, doping concentration on device performance were systematically investigated. The optimized structure used a 600 nm absorber, a 170 nm Nb_2O_5 electron

© 2026 The Authors. This article is an Open Access article distributed under the terms and conditions of the Creative Commons Attribution(CC–BY)license
https://creativecommons.org/licenses/by/4.0

transport layer, and a 110 nm Cu_2O hole transport layer, with doping concentrations of 1×10^{20} m^{-3} (absorber), 1×10^{21} m^{-3} (ETL), and 1×10^{24} m^{-3} (HTL), and an absorber defect density of 1×10^{19} m^{-3}. Performance decreased at higher defect densities because of trap-assisted recombination and declined at higher temperatures mainly because of a reduction in Voc, so 300 K gave the best result within the studied range. The optimized device achieved a power conversion efficiency of 10.29%, an open-circuit voltage of 1.62 V, a short-circuit current density of 10.39 mA/cm², and a fill factor of 61%. The high Voc is attributed to the wide band gap of $MAPbBr_3$ and the favorable band alignment with the Nb_2O_5 and Cu_2O layers. These simulation results show that Nb_2O_5 and Cu_2O are promising inorganic transport layers for proficient and stable wide-band-gap perovskite solar cells, and experimental validation is recommended as future work.

References

[1] Kojima, A., et al. (2009). Organometal halide perovskites as visible-light sensitizers for photovoltaic cells. Journal of the American Chemical Society, 131(17), 6050–6051.

[2] National Laboratory of the Rockies (NLR). (2026). Best Research-Cell Efficiency Chart. Retrieved October 25, 2026, from https://www.nlr.gov/pv/data-tools

[3] Nie, T., et al. (2023). Recent advances in wide-bandgap organic–inorganic halide perovskite solar cells and tandem application. Nano-Micro Letters, 15(1), 70.

[4] Tong, Y., et al. (2022). Wide-bandgap organic–inorganic lead halide perovskite solar cells. Advanced Science, 9(14), 2105085.

[5] Ferdowsi, P., et al. (2020). Ultrathin polymeric films for interfacial passivation in wide band-gap perovskite solar cells. Scientific Reports, 10(1), 22260.

[6] Ren, G., et al. (2021). Strategies of modifying spiro-OMeTAD materials for perovskite solar cells: A review. Journal of Materials Chemistry A, 9(8), 4589–4625.

[7] Yu, W., et al. (2016). Ultrathin Cu2O as an efficient inorganic hole transporting material for perovskite solar cells. Nanoscale, 8(11), 6173–6179.

[8] Feng, J., et al. (2017). E-beam evaporated Nb2O5 as an effective electron transport layer for large flexible perovskite solar cells. Nano Energy, 36, 1–8.

[9] MacKenzie, R. C., et al. (2012). Extracting microscopic device parameters from transient photocurrent measurements of P3HT:PCBM solar cells. Advanced Energy Materials, 2(6), 662–669.

[10] MacKenzie, R. C., et al. (2011). Modeling nongeminate recombination in P3HT:PCBM solar cells. The Journal of Physical Chemistry C, 115(19), 9806–9813.

[11] MacKenzie, R. C., et al. (2013). Interpreting the density of states extracted from organic solar cells using transient photocurrent measurements. The Journal of Physical Chemistry C, 117(24), 12407–12414.

[12] Almuqoddas, E., et al. (2024). Near fundamental limit performance of inverted perovskite solar cells with anti-reflective coating integration. Results in Optics, 16, 100670.

[13] Srivastava, V., et al. (2024). Investigation of eco-friendly perovskite solar cell employing niobium pentoxide as electron transport material using SCAPS-1D. Transactions on Electrical and Electronic Materials, 25(3), 294–303.

[14] Bouazizi, S., et al. (2024). Growth and efficiency of MAPbBr3 based perovskite solar cells: Insight from experimental and simulation. Indian Journal of Physics, 98(9), 3341–3353.

[15] Ismail, M., et al. (2023). Boosting efficiency of eco-friendly perovskite solar cell through optimization of novel charge transport layers. Royal Society Open Science, 10(6), 230331.

[16] Pazos-Outón, L. M., Xiao, T. P., & Yablonovitch, E. (2018). Fundamental efficiency limit of lead iodide perovskite solar cells. The Journal of Physical Chemistry Letters, 9(7), 1703–1711.

[17] Bag, A., et al. (2020). Effect of absorber layer, hole transport layer thicknesses, and its doping density on the performance of perovskite solar cells by device simulation. Solar Energy, 196, 177–182.

[18] Raavi, S. S. K. (2020). Ultrafast nonlinear optical properties and excited-state dynamics of Soret-band excited D-π-D porphyrins.

[19] Jan, S. T., & Noman, M. (2022). Influence of layer thickness, defect density, doping concentration, interface defects, work function, working temperature and reflecting coating on lead-free perovskite solar cell. Solar Energy, 237, 29–43.

[20] Abdi-Jalebi, M., et al. (2017). Dopaje de cationes monovalentes de CH3NH3PbI3 para células solares eficientes perovskita. Journal of Visualized Experiments (JoVE), (121), e55307.

[21] Gamal, N., et al. (2021). Design of lead-free perovskite solar cell using Zn1-xMgxO as ETL: SCAPS device simulation. Optik, 242, 167306.

[22] Ščajev, P., et al. (2022). Impact of dopant-induced band tails on optical spectra, charge carrier transport, and dynamics in single-crystal CdTe. Scientific Reports, 12(1), 12851.

[23] Adeleye, D., et al. (2021). Lifetime, quasi-Fermi level splitting and doping concentration of Cu-rich CuInS2 absorbers. Materials Research Express, 8(2), 025905.

© 2026 The Authors. This article is an Open Access article distributed under the terms and conditions of the Creative Commons Attribution(CC–BY)license
https://creativecommons.org/licenses/by/4.0